ILL Document Delivery

REG-14355362

MDUDLS

NLM -- W1 JO564T (Gen); E-Journal w/ILL access

Elizabeth Drexler
NIST
Boulder, CO 80305

ATTN:		SUBMITTED:	2008-03-04 15:54:56
PHONE:	301-975-3981	PRINTED:	2008-03-07 09:30:27
FAX:	303-497-5030	REQUEST NO.:	REG-14355362
E-MAIL:	drexler@boulder.nist.gov	SENT VIA:	DOCLINE
		DOCLINE NO.:	24365876

REG | Copy | Journal | NEED BEFORE: 2008-04-17

TITLE:	JOURNAL OF BIOMECHANICS
PUBLISHER/PLACE:	Elsevier Science New York Ny
VOLUME/ISSUE/PAGES:	2007;40(4):812-9 812-9
DATE:	2007
AUTHOR OF ARTICLE:	Drexler E;Quinn T;Slifka A;McCowan C;Bischoff J;Wright J;Ivy
TITLE OF ARTICLE:	COMPARISON OF MECHANICAL BEHAVIOR AMONG THE EXTRAP
ISSN:	0021-9290
OTHER NUMBERS/LETTERS:	Unique ID.: 0157375 24365876 16682044
SOURCE:	PubMed
COPYRIGHT COMP.:	Guidelines
CALL NUMBER:	W1 JO564T (Gen); E-Journal w/ILL access
NOTES:	48760
REQUESTER INFO:	Drexler, Elizabeth
DELIVERY:	E-mail: drexler@boulder.nist.gov
REPLY:	Mail:

KEEP THIS RECEIPT TO RECONCILE WITH BILLING STATEMENT
For problems or questions, contact NLM at http://wwwcf.nlm.nih.gov/ill/ill_web_form.cfm or phone 301-496-5511.
Include LIBID and request number.

ELSEVIER

Journal of Biomechanics 40 (2007) 812–819

JOURNAL OF BIOMECHANICS

www.elsevier.com/locate/jbiomech
www.JBiomech.com

Comparison of mechanical behavior among the extrapulmonary arteries from rats ☆

E.S. Drexler[a,*], T.P. Quinn[a], A.J. Slifka[a], C.N. McCowan[a], J.E. Bischoff[b], J.E. Wright[a], D.D. Ivy[c], R. Shandas[c,d]

[a]*Materials Reliability Division (MS 853), National Institute of Standards and Technology, 325 Broadway, Boulder, CO 80305, USA*
[b]*Department of Mechanical Engineering, University of South Carolina, Columbia, SC 29208, USA*
[c]*Department of Pediatrics, Section of Cardiology, University of Colorado Health Sciences Center, Denver, CO 80218, USA*
[d]*Department of Mechanical Engineering, University of Colorado, Boulder, CO 80309, USA*

Accepted 13 March 2006

Abstract

Results of comparative tests on pulmonary arteries from untreated Long Evans rats are presented from three sections of the artery: the trunk, and the right and left main extrapulmonary arteries. Analyses were conducted looking for mechanical differences between the flow (longitudinal) and circumferential directions, between the right and left main arteries, and between each of the mains and the trunk. The mechanical properties of rat pulmonary arteries were obtained with a bubble inflation technique. A flat disk of rat pulmonary artery was constrained at the periphery and inflated, and the geometry of the resulting bubble of material recorded from six different angles. To analyze the data, the area under the stress–strain curve was calculated for each test and orientation. This area, related to the strain-energy density, was calculated at stress equal to 200 kPa, for the purpose of statistical comparison. The mean values for the area show that the trunk is less compliant than the main arteries; this difference is supported by histological evidence. When comparing the circumferential and longitudinal properties of the arteries, differences are found for the trunk and left main arteries, but with opposite orientations being more compliant. The mean values for the two orientations for the right main artery are statistically identical. There was indication of significant difference in mechanical properties between the trunk and the main arteries. The left main artery in the circumferential orientation is highly compliant and appears to strongly influence the likelihood that significant differences will exist when included in a statistical population. These data show that each section of the extrapulmonary arterial system should not be expected to behave identically, and they provide the baseline mechanical behavior of the pulmonary artery from normotensive rats.

Keywords: Bubble test; Mechanical properties; Pulmonary arteries; Pulmonary hypertension; Stress; Strain

1. Introduction

Individuals with pulmonary hypertension (PH), either idiopathic or otherwise, can develop stiffening of the proximal pulmonary arteries subsequent to changes in downstream pulmonary vascular resistance. Consequences of PH are increased workload on the right ventricle as well as functional and structural alterations of the pulmonary vasculature (Humbert et al., 2004). There are several studies being conducted to evaluate molecular, cellular, and mechanical factors influencing downstream pulmonary arteries, but detailed biomechanical studies of the proximal arteries are lacking. These arteries are known to be more than simply passive conduits to move blood into the pulmonary microcirculation; they play key roles in

☆ Contribution of the National Institute of Standards and Technology, an agency of the US government; not subject to copyright in the USA.

*Corresponding author. Tel.: +1 303 497 5350; fax: +1 303 497 5030.
E-mail address: drexler@boulder.nist.gov (E.S. Drexler).

0021-9290/$ - see front matter © 2006 Elsevier Ltd. All rights reserved.
doi:10.1016/j.jbiomech.2006.03.010

modulating pulmonary hemodynamics (Heath et al., 1959; Hoffman, 1972; Ramsey and Jones, 1994; Sniderman and Fitchett, 1988; Tozzi et al., 1994). Understanding the fundamental biomechanical features of these arteries under normal and hypertensive conditions becomes an important component in assembling a complete picture of pulmonary vascular dynamics in PH. Such information should also facilitate the development of novel diagnostic techniques for evaluation of the mechanics of the proximal pulmonary artery in the clinical situation.

A rat model is a common first step in understanding diseases such as PH. This study characterizes the mechanical properties with respect to structure of all the extrapulmonary arteries—those more accessible in the clinical setting—in both the circumferential direction and direction of blood flow to establish baseline properties for comparison with hypertensive arteries. Several studies have examined structural and mechanical changes to the rat pulmonary arteries with hypertension. However, the lack of data on the proximal trunk and main extrapulmonary arteries limit the utility of the data presented in these studies for our investigation of the mechanics of proximal arteries.

It has been established that the lung and pulmonary arteries remodel with PH (Fung and Liu, 1991; Jeffery and Morrell, 2002; Meyrick and Reid, 1980), and the changes occurring in the lung have been well characterized (Altiere et al., 1986; Davies and Reid, 1991; Ivy et al., 2005; Langleben et al., 1988; McKenzie et al., 1984; Meyrick and Reid, 1981; Wilson et al., 1989). However, the pathology and, particularly, the mechanics of the pulmonary trunk and the extrapulmonary arteries are less well documented. McKenzie et al. (1984) have reported on the biochemical and histological response of the pulmonary trunk to hypoxia-induced PH, and Wilson et al. (1989) described the pathology of monocrotaline-induced PH in the "major pulmonary arteries." A few research groups (Coflesky et al., 1987; Huang et al., 2001; Langleben et al., 1988; Liu and Fung, 1993a b; Liu, 1996) have examined the mechanics of the left extra- and intrapulmonary main arteries, but none have studied the mechanical properties of the trunk or compared properties of the right and left main extrapulmonary arteries. Only Liu and Fung (1993a, b) have compared the circumferential and longitudinal (direction of blood flow) orientations. Using a mouse model, the circumferential mechanical properties have been measured in the left main pulmonary artery and have correlated the measured properties to the structure of the normal (Chesler et al., 2004) and hypertensive (Kobs et al., 2005) arterial wall.

Based on a review of past studies (Debes and Fung, 1995, Holzapfel et al., 2000; Humphrey et al., 1993), we chose to use the bubble test for our studies. In research led by Humphrey (Downs et al., 1990; Hsu et al., 1994, 1995; Humphrey et al., 1987), the bubble test technique was refined to account for the anisotropy of the displacements with loading and resulted in a two-dimensional strain energy function. The bubble test provides a good compromise between the increased complexity (and resulting decrease in experimental reproducibility) of a full tension/inflation/torsion test and the simplicity (and potential lack of accuracy) of a basic uniaxial test. Furthermore, the test is efficient to set up and run, it is well-suited for small samples, the circumferential and longitudinal data are readily obtainable, and the choice of the bubble test is justified by the membrane-type characteristics of the highly compliant pulmonary arterial wall. Recognizing that the bubble test does not allow for a comprehensive analysis of the artery properties, it does however provide for comparisons of sections and orientations not readily available from other test configurations.

2. Materials and methods

2.1. Specimen preparation

Animal studies were performed following institutional guidelines and an approved protocol (ASP # 44404004(07)1E). The rat pulmonary arteries used for mechanical testing were from Long–Evans rats with ages ranging from 83 to 89 days. The rats were sacrificed at University of Colorado Health Sciences Center, where the extrapulmonary arteries were dissected away from surrounding lung and thoracic tissue. The artery was transported in isotonic buffered solution (RPMI[1]) for mechanical testing. All tests were conducted within 24 h of sacrifice.

The arteries were first visually inspected for anomalies (holes, tears, extraneous material, etc.), then each artery was further prepared to provide three test specimens per animal—one each from the trunk, right main artery, and left main artery. Each section was cut parallel to its axis and opened to form a rectangular piece of tissue. A reference line was marked on the material with India ink, indicating the direction of blood flow through the artery, and the adventitial layer was trimmed to obtain uniform thickness and provide a specimen for testing that consisted primarily of the medial layer (bound by the inner and outer elastic lamina, and the intima). A circular disk (~3 mm in diameter) was cut for placement into the test fixture from the rectangle. The test specimen was then placed intima side up on an O-ring and loaded into the fixture with the flow (longitudinal) direction of the specimen lined up with the pressure inlet tube of the test fixture. Care was taken to avoid

[1]Product name is provided only for completeness of description. Its inclusion does not imply endorsement by NIST.

prestressing the specimen during this procedure. For the duration of the test, the test fixture was placed in a reservoir of phosphate-buffered saline solution (without Ca or Mg) held at 37 °C.

2.2. Experimental setup

The specifics of the experimental setup are described elsewhere (Drexler et al., 2003). Fig. 1 shows a schematic drawing of the test fixture. In order for membrane assumptions to be applicable to this bubble-inflation test, the general rule is that the diameter of the sample (or the aperture through which it is inflated) be at least 10 times the thickness of the sample (Young and Budynas, 2002). The aperture in the cap of the test fixture is 2.318 mm in diameter and for the pulmonary arteries tested, the thickness of the specimen was generally less than 0.200 mm.

The cylindrical tank was designed with twelve equally spaced windows at 30° intervals through which the specimen may be viewed. A set of six images was taken of the inflated material by three cameras, 60° apart, and with a rotating stage. Commercially available computer software was used to incrementally increase pressure every 1.38 kPa. A review of the literature showed that mean pulmonary arterial pressure (mPAP) in healthy rats can range from 2.57 kPa (Jiang et al., 2002) in Sprague–Dawley rats to 3.84 kPa (Deten et al., 2003) in Long-Evans rats. A maximum inflation pressure of 17.9 kPa was chosen to mimic extreme hypertension in the pulmonary artery. Fig. 2 shows a schematic of the test system. All elements of the pressurization system had low compliance relative to the test material, and the range of pressure was adequate for testing of the compliant arteries, with minimal pressure hysteresis. The thickness of each specimen was measured after the test with a laser micrometer.

2.3. Analytical approach

Images collected from the horizontal cameras were used to determine response in the circumferential C (0°)

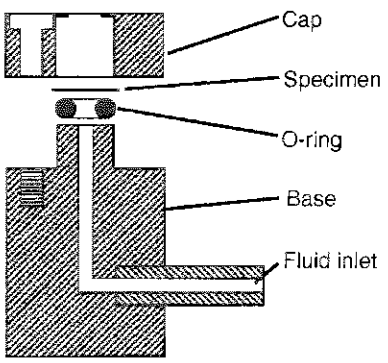

Fig. 1. Schematic of the bubble test fixture.

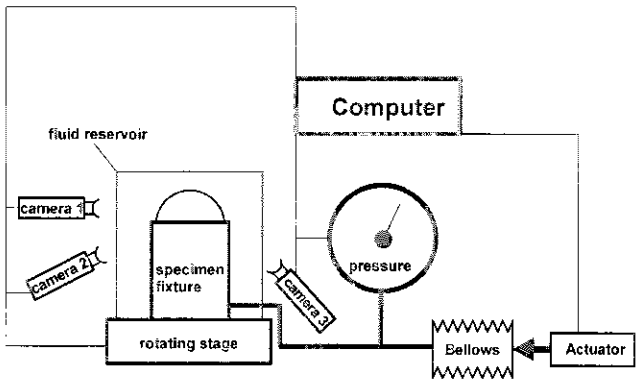

Fig. 2. Schematic of the computer-controlled bubble test system.

and longitudinal L (90°) orientations. Average strain ε for each orientation was calculated from the length l (uncertainty $u_l = 0.058$ mm) of the inflated material (profile) at each pressure p ($u_p = 0.195$ kPa) increment, and relative to a calculated initial length l_0. The initial portion of the length vs. pressure l-p data (1.38–6.90 kPa) was fit to a straight line and the intercept at $p = 0$ was used for l_0. The stretch λ was calculated relative to the length l_0:

$$\lambda_{C,L} = \frac{l}{l_0}, \tag{1}$$

$$\varepsilon = \ln \lambda_{C,L}. \tag{2}$$

We will make the standard assumptions that the material is incompressible, pseudoelastic, anisotropic, homogeneous, and can be modeled as a membrane (Fung, 1993). The strain is not uniform in the inflated ellipsoid because the stress in an ellipsoid under internal pressure varies with spatial location and direction and the anisotropic nature of the arterial tissue. We are reporting the average strain based on the entire length of the bubble profile to reduce the noise in the measurement of strain. To understand the magnitude of the variation one expects in the strain, we modeled a representative test (a left artery which demonstrates the most strain-stiffening behavior observed and is a worst case) with the constitutive law proposed in Bischoff et al. (2004). The model parameters were found by minimizing the difference between the model-predicted final shape using finite elements and that measured in the experiments at the maximum pressure. For the sample fitted, the model predicted that the difference between the average strain and the strain at the crown of the bubble was 5%.

For stress, the arterial wall was assumed to be incompressible permitting calculation of the material thickness t ($u_t = 0.0172$ mm) from the surface area of the inflated material. The surface area was approximated as a partial general ellipsoid. The vertical semi-axis (c) ($u_c = 0.029$ mm) and the horizontal semi-axes (a and b)

of the ellipsoid were determined by examining the side-view images. The semi-axes a and b ($u_{a,b} = 0.014$ mm) of the ellipsoid did not necessarily align with the circumferential and longitudinal orientations (Fig. 3a). The off-axis angle θ was obtained by measuring the width of the bubble at the end of the test for all camera angles to determine the orientation of the horizontal minor axis. The actual values for the semi-axes a and b were calculated from θ and the projection of the semi-axes in the circumferential and longitudinal views, a' and b', respectively. When $\theta = 0$, $a' = a$ and $b' = b$. Given θ, a', and b', the semi-axes of the ellipsoid, a and b, were calculated from

$$a = \sqrt{\frac{a'^2 - b'^2\tan^2\theta}{1-\tan^2\theta}} \quad \sqrt{\frac{b'^2 - a'^2\tan^2\theta}{1-\tan^2\theta}}. \tag{3}$$

The surface area S of each bubble was then numerically expressed as the surface area of a partial ellipsoid, with h representing the offset of the center of the ellipsoid from the base (i.e., flat bottom) of the bubble. Fig. 3 shows schematically how S would appear for $h>0$ (Fig. 3b) and for $h<0$ (Fig. 3c).

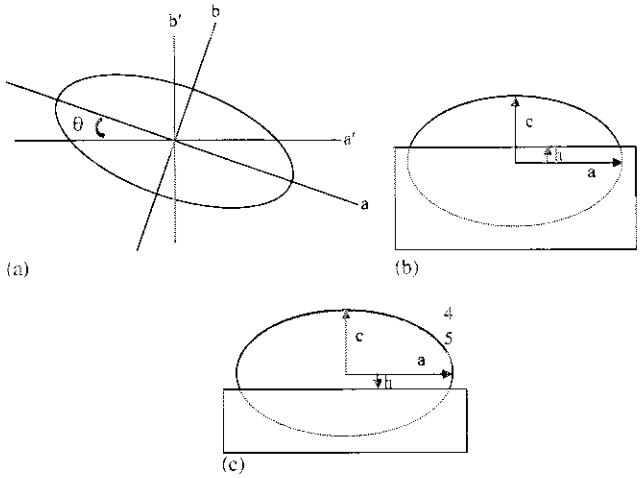

Fig. 3. Schematics showing the off-axis angle θ from the top view of the ellipsoid (a), the side view when $0 \leqslant h < c$ (b), and the side view when $h<0$ (c).

As expressed by Flugge (1973), the maximum stresses at the top of a general ellipsoidal shell under internal pressure are given by

$$\sigma_L = \frac{pc}{2t}\left[\frac{ab}{c^2} - \left(\frac{a}{b} - \frac{b}{a}\right)\cos 2\theta^*\right]\sqrt{\frac{b^2 + (a^2 - b^2)\cos^2\theta^*}{a^2 + (b^2 - a^2)\cos^2\theta^*}} \tag{4}$$

and

$$\sigma_C = \frac{pc}{2t}\left[\frac{ab}{c^2} - \left(\frac{a}{b} - \frac{b}{a}\right)\cos 2\theta^*\right]\sqrt{\frac{a^2 + (b^2 - a^2)\cos^2\theta^*}{b^2 + (a^2 - b^2)\cos^2\theta^*}}, \tag{5}$$

where σ_L and σ_C are the Cauchy stresses in the longitudinal and circumferential directions, respectively, and θ^* is found from the relation

$$\tan\theta = \frac{a}{c}\tan\theta^*. \tag{6}$$

The initial load (0 kPa) was defined as the point where the tissue continued emerging above the surface of the fixture without increasing the pressure ; that is, $\Delta\delta > 0$ when $\Delta p = 0$, where δ is displacement.

3. Results

Bubble tests were conducted on specimens from eight untreated rats. Representative images looking at deformation at 17.9 kPa in the circumferential and longitudinal orientations are shown in Fig. 4a and b, respectively. From images and the pressures at which they were collected, mechanical properties for the arteries were calculated. Data showing the maximum stress as a function of average strain, comparing the

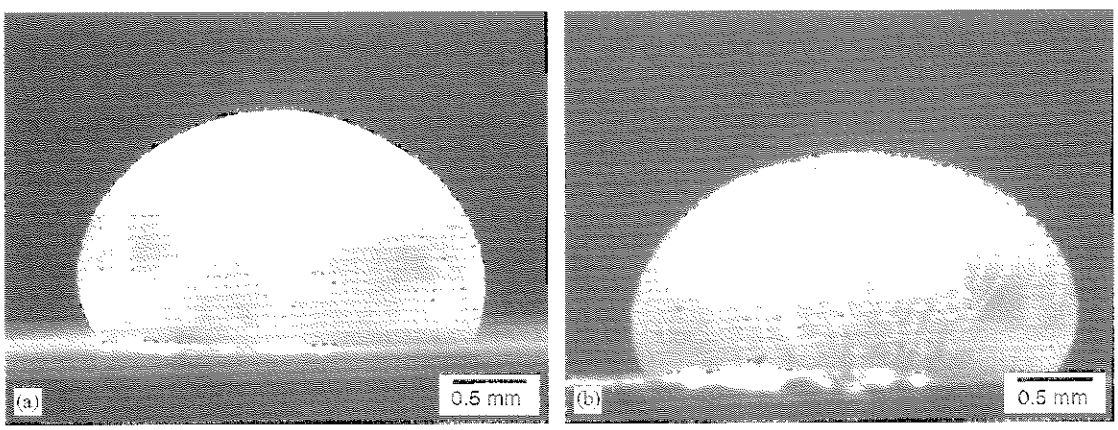

Fig. 4. Side-view images of a fully inflated trunk and looking in the direction of (a) circumferential (0° camera) and (b) longitudinal (90° camera) displacements.

circumferential and longitudinal orientations, are in Fig. 5a–c for the trunk, the right main artery, and the left main artery, respectively, from all tests. One major observation from these plots is that the right and left main arteries demonstrate strain-stiffening behavior, where the maximum stress increases sharply with little increase in strain, unlike the trunks. The mean thickness of the trunks is 40% higher than the mean thickness of the main arteries, so the same pressures resulted in lower stresses for the trunks as compared with the main arteries. It also appears that the right main shows less strain than the left main. The relationship between the longitudinal and circumferential orientations for each section is not clear from the plots.

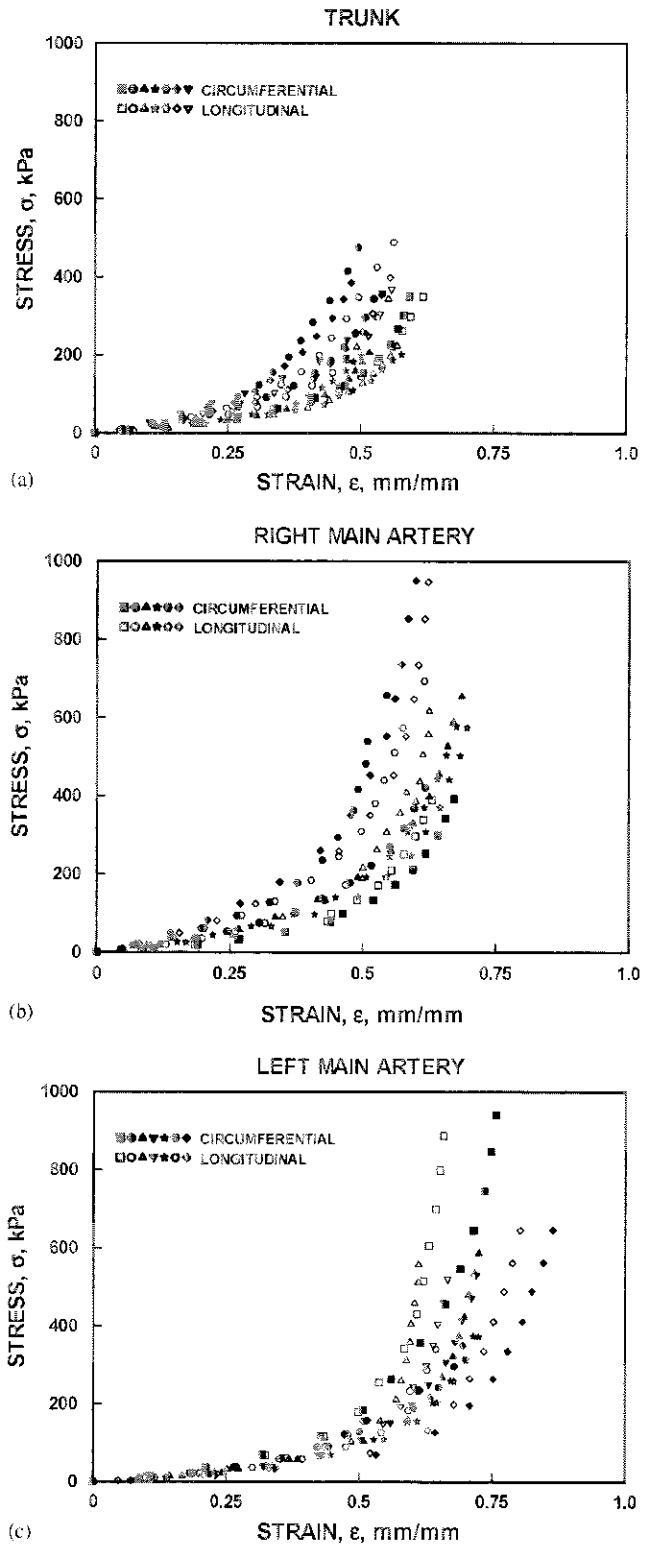

Fig. 5. Plots showing the relationship between stress and average strain in the (a) trunk, (b) right, and (c) left main arteries. Different symbols correspond to each artery tested.

We fit each stress–strain curve, in the longitudinal and circumferential orientations, with a spline and integrated under the curve to obtain a value that could be used for statistical comparison. The integration limits were from 0 to 200 kPa, the largest stress achieved by all the tests. This calculated area A is related monotonically to the strain-energy density for that orientation, and the greater the value of A, the more compliant the artery.

The data were analyzed to determine whether a significant difference existed in A between any two conditions. (In anticipation of comparing these data with the data from rats treated to induce PH, we will present all statistical comparisons that are of potential interest.) Table 1 provides the mean and standard deviation of A for each section and orientation. Table 2 shows the statistical comparison of the two conditions indicated; the first column lists the two conditions being compared. The first letter indicates the section (L = left main, R = right main, T = trunk), the second letter indicates orientation (L = longitudinal, C = circumferential). The second column contains the values for probability P as determined by Student's T test (or a paired T test, where indicated). A paired T test was employed when there was a direct comparison between two orientations from the same artery. Because we did not obtain valid results (due to leaks during the test or flaws) for every section of every artery it was not possible to compare the sections using the paired T test.

Table 1
Values for the mean and standard deviation of A calculated at $\sigma = 200$ kPa

Section/orientation	A
LL	31.9±2.2
LC	35.3±2.3
RL	32.0±2.6
RC	32.2±2.8
TL	30.4±2.6
TC	28.2±4.2

The first letter indicates the section (L = left main, R = right main, T = trunk), the second letter indicates orientation (L = longitudinal, C = circumferential).

4. Histology

A histological study of untreated rat PAs was conducted in order to better understand the results of our mechanical tests and to provide a baseline for future tests on treated animals. We observed that the trunks of the pulmonary arteries characteristically have more layers of elastic laminae than do the left and right main arteries, as shown in Fig. 6a and b. Here, the trunk is bounded by internal and external elastic lamina and has about eight internal laminae, with average thicknesses of about 4 μm. The overall thickness of the medial layer shown for this trunk is about 90 μm. The main artery shown in Fig. 6b is bound by internal and external elastic lamina and has about 5 internal laminae, of similar thicknesses. The overall thickness of this main is about 70 μm. The areal fraction of the laminae in these two cases was measured to be 50% and 35% for the trunk and main, respectively. The higher areal fraction (and presumably volume fraction) of elastin found in the trunk would support the significantly different mechanical behavior observed between the trunk and main arteries.

The right and left main arteries also have characteristic differences. The right main typically has a larger diameter and is shorter (between heart and lung) than the left main. The thicknesses of the media in the right main range from 50 to 150 μm, and have 3–6 internal elastic laminae. The left main artery is generally thinner than the right main artery, about 50–90 μm, with 2–3 internal elastic laminae.

Table 2
P-values as determined from Student's *T* test for A calculated at $\sigma = 200$ kPa

	P
M vs. T	9.60E-04
L vs. T	1.40E-03
R vs. T	0.033
L vs. R	0.16
MC vs. TC	0.0022
ML vs. TL	0.19
LC vs. TC	2.00E-03
RC vs. TC	0.074
LL vs. TL	0.26
RL vs. TL	0.3
LC vs. RC	0.048
LL vs. RL	0.96
LL vs. LC*	0.0093
RL vs. RC*	0.86
TL vs. TC*	0.041

*Paired *T*-test: $P<0.05$.
The first letter indicates the section (L = left main, R = right main, T = trunk), the second letter indicates orientation (L = longitudinal, C = circumferential).

5. Discussion

The data for *A* indicate that the left main artery in the circumferential orientation is the most compliant, the trunk in the circumferential orientation is the least, and both orientations of the right main artery fall between (Table 1). Significant differences (Table 2) exist between the trunk and pooled population from both main arteries ($P<0.001$), and the left ($P<0.005$) and right ($P<0.05$) independently. No significant differences appear when comparing the right and left main arteries ($P>0.1$). Looking at the contribution of the orientation, indications are that the circumferential orientation from the left main artery is significantly more compliant than anything to which it is compared. Comparisons between the different orientations from the right main artery and the trunk reveal no significant differences, nor do they appear to exist between the left longitudinal and either the right or trunk in the longitudinal orientation.

Comparison between the longitudinal and circumferential orientations for each section seems to show significant differences for the trunk ($P<0.05$) and left

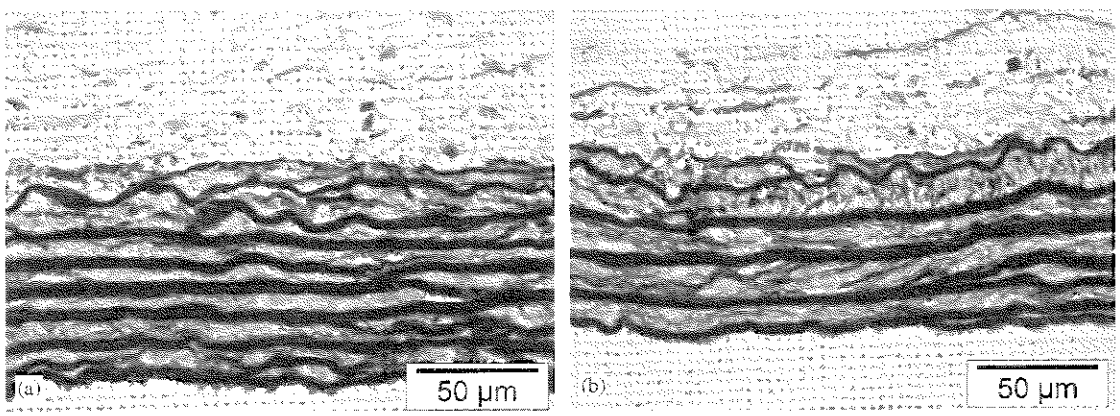

Fig. 6. Cross-sectional views of (a) trunk and (b) right main extrapulmonary artery from an untreated rat with adventitia left untrimmed. Note the greater number of elastic laminae visible in the dark gray medial layer for the trunk vs. the main extrapulmonary artery. The stain is pentachrome.

main artery ($P<0.01$), but not for the right ($P>0.5$). A is consistently greater in the circumferential orientation for the left main artery, and predominantly greater in the longitudinal orientation for the trunk when making a direct comparison between orientations. There is no predominance in the right main artery.

The reason for these differences has yet to be determined. Simple structural differences, such as proximity to feeder arteries or bifurcations in the longitudinal direction, may account for an apparent statistical difference between the circumferential and longitudinal orientations. But perhaps there are other factors; the rat physiology shows that the left lung has a single lobe, whereas the right has four major lobes and one minor. The artery supplying the right lung is shorter with a larger diameter, whereas the left is longer, narrower and straighter. Theoretically, the narrower left main artery would need to transport the same volume of blood as the larger diameter right main artery, so it would need to be more compliant to accommodate the volume. Clearly different transport functions (conduit vs. dampening functions) contribute to the different properties of the trunk and the left main artery.

Acknowledgments

Portions of this work performed at the University of Colorado Health Sciences Center (UCHSC) were supported by a grant from the NIH (HL 67393). The authors are indebted to K. Colvin of UCHSC for preparing rats and excising pulmonary arteries. Discussions with K. Coakley, J. Splett, and D. Vecchia of the Statistical Engineering Division at NIST, are gratefully acknowledged.

References

Altiere, R.J., Olson, J.W., Gillespie, M.N., 1986. Altered pulmonary vascular smooth muscle responsiveness in monocrotaline-induced pulmonary hypertension. Journal of Pharmacology and Experimental Therapeutics 236, 390–395.

Bischoff, J.E., Arruda, E.M., Grosh, K., 2004. A rheological network model for the continuum anisotropic and viscoelastic behavior of soft tissue. Biomechanics and Modeling in Mechanobiology 3, 56–65.

Chesler, N.C., Thompson-Figueroa, J., Millburne, K., 2004. Measurements of mouse pulmonary artery biomechanics. Journal of Biomechanical Engineering 126, 309–314.

Coflesky, J.T., Jones, R.C., Reid, L.M., Evans, J.N., 1987. Mechanical properties and structure of isolated pulmonary arteries remodeled by chronic hyperoxia. American Review of Respiratory Diseases 136, 388–394.

Davies, P., Reid, L., 1991. Hypoxic remodeling of the rat pulmonary arterial microcirculation assessed by microdissection. Journal of Applied Physiology 71, 1886–1891.

Debes, J.C., Fung, Y.C., 1995. Biaxial mechanics of excised canine pulmonary arteries. American Journal of Physiology 269, H433-H442.

Deten, A., Millar, H., Zimmer, H.-G., 2003. Catheterization of pulmonary artery in rats with an ultraminiature catheter pressure transducer. American Journal of Physiology—Heart and Circulatory Physiology 285, H2212–H2217.

Downs, J., Halprin, H.R., Humphrey, J., Yin, F., 1990. An improved video-based computer tracking system for soft biomaterials testing. IEEE Transactions on Biomedical Engineering 37, 903–907.

Drexler, E.S., Slifka, A.J., Wright, J.E., McCowan, C.N., Finch, D.S., Quinn, T.P., McColskey, J.D., Ivy, D.D., Shandas, R., 2003. An experimental method for measuring mechanical properties of rat pulmonary arteries verified with latex. Journal of Research of the National Institute of Standards and Technology 108, 183–191.

Flugge, W., 1973. Stresses in Shells. Springer, New York.

Fung, Y.C., 1993. Biomechanics Mechanical Properties of Living Tissues, second ed. Springer, New York.

Fung, Y.C., Liu, S.Q., 1991. Changes of zero-stress state of rat pulmonary arteries in hypoxic hypertension. Journal of Applied Physiology 70, 2455–2470.

Heath, D., Wood, E., DuShane, J., Edwards, J.E., 1959. The structure of the pulmonary trunk at different ages and in cases of pulmonary hypertension and pulmonary stenosis. Journal of Pathology and Bacteriology 77, 443–456.

Hoffman, J., 1972. Diagnosis and treatment of pulmonary vascular disease. Birth Defects 8, 9–18.

Holzapfel, G.A., Gasser, T.C., Ogden, R.W., 2000. A new constitutive framework for arterial wall mechanics and a comparative study of material models. Journal of Elasticity 61, 1–48.

Hsu, F.P.K., Schwab, C., Rigamonti, D., Humphrey, J.D., 1994. Identification of response functions from axisymmetric membrane inflation tests: implications for biomechanics. International Journal of Solids and Structures 31, 3375–3386.

Hsu, F.P.K., Liu, A.M.C., Downs, J., Rigamonti, D., Humphrey, J.D., 1995. A triplane video-based experimental system for studying axisymmetrically inflated biomembranes. IEEE Transactions on Biomedical Engineering 42, 442–450.

Huang, W., Delgado-West, D., Wu, J.T., Fung, Y.C., 2001. Tissue remodeling of rat pulmonary artery in hypoxic breathing. I. Changes of morphology, zero-stress state, and gene expression. Annals of Biomedical Engineering 29, 535–551.

Humbert, M., Morrell, N.W., Archer, S.L., Stenmark, K.R., MacLean, M.R., Lang, I.M., Christman, B.W., Weir, E.K., Eickelberg, O., Voelkel, N.F., Rabinovitch, M., 2004. Cellular and molecular pathobiology of pulmonary arterial hypertension. Journal of the American College of Cardiology 43 (Suppl. S), 13S–24S.

Humphrey, J.D., Vawter, D.L., Vito, R.P., 1987. Quantification of strains in biaxially tested soft tissues. Journal of Biomechanics 20, 59–65.

Humphrey, J.D., Kang, T., Sakarda, P., Anjanappa, M., 1993. Computer-aided vascular experimentation: a new electromechanical test system. Annals of Biomedical Engineering 21, 33–43.

Ivy, D.D., McMurtry, I.F., Colvin, K., Imamura, M., Oka, M., Lee, D.-S., Gebb, S., Jones, P.L., 2005. Development of occlusive neointimal lesions in distal pulmonary arteries of endothelin B receptor-deficient rats. Circulation 111, 2988–2996.

Jeffery, T.K., Morrell, N.W., 2002. Molecular and cellular basis of pulmonary vascular remodeling in pulmonary hypertension. Progress in Cardiovascular Diseases 45, 173–202.

Jiang, B.H., Maruyama, J., Yokochi, A., Amano, H., Mitani, Y., Mauyama, K., 2002. Correlation of inhaled nitric-oxide induced reduction of pulmonary artery pressure and vascular changes. European Respiratory Journal 20, 52–58.

Kobs, R.W., Muvarak, N.E., Eickhoff, J.C., Chesler, N.C., 2005. Linked mechanical and biological aspects of remodeling in mouse pulmonary arteries with hypoxia-induced hypertension. American Journal of Physiology—Heart and Circulatory Physiology 288, H1209–H1217.

Langleben, D., Szarek, J.L., Coflesky, J.T., Jones, R.C., Reid, L.M., Evans, J.N., 1988. Altered artery mechanics and structure in monocrotaline pulmonary hypertension. Journal of Applied Physiology 65, 2326–2331.

Liu, S.Q., 1996. Alterations in structure of elastic laminae of rat pulmonary arteries in hypoxic hypertension. Journal of Applied Physiology 81, 2147–2155.

Liu, S.Q., Fung, Y.C., 1993a. Changes in the structure and mechanical properties of pulmonary arteries of rats exposed to cigarette smoke. American Review of Respiratory Diseases 148, 768–777.

Liu, S.Q., Fung, Y.C., 1993b. Material coefficients of the strain energy function of pulmonary arteries in normal and cigarette-exposed rats. Journal of Biomechanics 26, 1261–1269.

McKenzie, J.C., Clancy Jr., J., Klein, R.M., 1984. Autoradiographic analysis of cell proliferation and protein synthesis in the pulmonary trunk of rats during the early development of hypoxia-induced pulmonary hypertension. Blood Vessels 21, 80–89.

Meyrick, B., Reid, L., 1980. Hypoxia-induced structural changes in the media and adventitia of the rat hilar pulmonary artery and their regression. American Journal of Pathology 100 (1), 151–178.

Meyrick, B., Reid, L., 1981. The effect of chronic hypoxia on pulmonary arteries in young rats. Experimental Lung Research 2, 257–271.

Ramsey, M.W., Jones, C.J.H., 1994. Large arteries are more than passive conduits. British Heart Journal 72, 3–4.

Sniderman, A.D., Fitchett, D.H., 1988. Vasodilators and pulmonary hypertension: the paradox of therapeutic success and clinical failure. International Journal of Cardiology 20, 173–181.

Tozzi, C.A., Christiansen, D.L., Poiani, G.J., Riley, D.J., 1994. Excess collagen in hypertensive pulmonary arteries decreases vascular distensibility. American Journal of Respiratory and Critical Care Medicine 149, 1317–1326.

Wilson, D.W., Segall, H.J., Pan, L.C., Dunston, S.K., 1989. Progressive inflammatory and structural changes in the pulmonary vasculature of monocrotaline-treated rats. Microvascular Research 38, 57–80.

Young, W.C., Budynas, R.G., 2002. Roark's Formulas for Stress and Strain, seventh ed. McGraw-Hill Companies, Inc., New York.